

Predominance of inhalation route in short-range transmission of respiratory viruses: Investigation based on computational fluid dynamics

Wenzhao Chen¹, Li Liu², Jian Hang³, Yuguo Li^{1,4} (✉)

1. Department of Mechanical Engineering, The University of Hong Kong, Pokfulam Road, Hong Kong, China

2. Department of Building Science, Tsinghua University, Beijing 100084, China

3. School of Atmospheric Sciences, Sun Yat-sen University, and Southern Marine Science and Engineering Guangdong Laboratory (Zhuhai), Zhuhai 519082, China

4. Faculty of Architecture, The University of Hong Kong, Pokfulam Road, Hong Kong, China

Abstract

During the coronavirus disease 2019 pandemic, short-range virus transmission has been observed to have a higher risk of causing infection than long-range virus transmission. However, the roles played by the inhalation and large droplet routes cannot be distinguished in practice. A recent analytical study revealed the predominance of short-range inhalation over the large droplet spray route as causes of respiratory infections. In the current study, short-range exposure was analyzed via computational fluid dynamics (CFD) simulations using a discrete phase model. Detailed facial membranes, including eyes, nostrils, and a mouth, were considered. In CFD simulations, there is no need for a spherical approximation of the human head for estimating deposition nor the “anisokinetic aerosol sampling” approximation for estimating inhalation in the analytical model. We considered two scenarios (with two spheres [Scenario 1] and two human manikins [Scenario 2]), source–target distances of 0.2 to 2 m, and droplet diameters of 3 to 1,500 μm . The overall CFD exposure results agree well with data previously obtained from a simple analytical model. The CFD results confirm the predominance of the short-range inhalation route beyond 0.2 m for expiratory droplets smaller than 50 μm during talking and coughing. A critical droplet size of 87.5 μm was found to differentiate droplet behaviors. The number of droplets deposited on the target head exceeded those exposed to facial membranes, which implies a risk of exposure through the immediate surface route over a short range.

1 Introduction

Since the beginning of the coronavirus disease 2019 (COVID-19) pandemic, the transmission mechanisms of respiratory viruses—particularly those of severe acute respiratory syndrome coronavirus 2 (SARS-CoV-2), which causes COVID-19—have become significantly clearer. The importance of the airborne or inhalation route for the transmission of SARS-CoV-2 was partly recognized by the World Health Organization in July 2020 (WHO 2020a). Airborne transmission involves the exhalation of fine, virus-laden, airborne respiratory droplets by an infected

person and the subsequent inhalation of the droplets by a susceptible person (Li 2021). Inhalation can occur at both short- and long-ranges, and short-range and long-range airborne transmission of SARS-CoV-2 was recognized in December 2021 (WHO 2021). Several COVID-19 outbreaks that were probably caused by airborne transmission have been reported (e.g., Miller et al. 2021; Li et al. 2021; Ou et al. 2022), and Banik and Ulrich (2020) reported evidence of short-range aerosol transmission.

Chen et al. (2022) established a link between short- and long-range airborne transmission. They concluded that a normally short-range-only disease can be transmitted over

Keywords

airborne transmission;
close contact;
short-range inhalation;
large droplet spray;
computational fluid dynamics

Article History

Received: 23 August 2022

Revised: 19 November 2022

Accepted: 25 November 2022

© Tsinghua University Press 2022

a long range in an overcrowded place with poor ventilation. Li et al. (2022b) also developed a simple continuum model that suggested that a continuum exists between the short- and long-range airborne routes. The authors showed that ventilation affects the infection risk in both short- and long-range airborne exposure events. Between any two people, the exposure risk due to inhalation or airborne transmission routes is greater at close range than at longer ranges. Liu et al. (2017) demonstrated this via both laboratory experiments and computational fluid dynamics (CFD) simulations considering only airborne exposure.

The analysis of short-range exposure is the cornerstone for setting physical distancing guidelines. Short-range exposure is not limited to inhalation. Two other possible short-range exposure routes are large droplet (or drop spray) transmission and the immediate surface route. Large-droplet or droplet transmission (Li 2021) involves the expulsion of virus-laden respiratory droplets from an infected person and the subsequent deposition of these droplets on the mucosal surfaces (e.g., eyes, nose, and mouth) of a susceptible person. For a long time, large droplet transmission has been suspected to be the dominant route in short-range scenarios resulting in respiratory infection. Large droplet transmission was also suspected to be the dominant transmission route in the early phase of the COVID-19 pandemic (WHO 2020b). Belief in the predominance of the large droplet route unfortunately led to an over-reliance on so-called droplet precautions. In the immediate surface route (Zhang et al. 2020a), expiratory droplets first deposit on the face or other body surfaces of a susceptible individual, who then touches the deposited droplets and thereafter immediately touches his/her mucosal surfaces, resulting in self-inoculation.

There have been few studies on the relative importance of these three transmission routes (i.e., inhalation, spray, and immediate surface touching) at short ranges. The exposure to expiratory droplets at a short range between two people can be influenced by the expired air speed of the infected individual, the phase difference between exhalation by the infected individual and inhalation by the susceptible individual, their body plumes and the buoyancy effect related to the height difference between them, and droplet size and distance. Chen et al. (2020) developed an analytical model of droplet inhalation and deposition. The authors approximated heads as spheres so that the existing formulas of deposition efficiency as a function of the Stokes number could be used for analysis. Moreover, they assumed inhalation exposure to be an aerosol sampling phenomenon, as the expired flow streamlines first diverged when approaching the mouth sampler and then converged into the mouth orifice. These limitations may be relaxed using CFD simulations, as CFD is a powerful approach that can provide more information

for studying short-range exposure and at a lower cost than experimental approaches. For the study of large-droplet exposure, detailed information on facial membrane exposure is important; however, this information is lacking in previous studies (Mui et al. 2009; Liu et al. 2022; Li et al. 2022a). Investigating short-range exposure is necessary for validating theoretical models and providing more insights that cannot be easily captured in an analytical model or experiments.

In this study, CFD was applied to simulate a range of interpersonal distances and droplets were tracked to investigate short-range exposure. Thermal manikins with detailed facial membranes, including eyes, nostrils, and a mouth, were used.

2 Methods

2.1 Case settings

In simulations, there are two major settings to consider. The first is the room setting (Figure 1), in which the effect of background airflows that surround two people need to be minimized. We considered a rectangular room with dimensions of 5 m (length) \times 5 m (width) \times 3 m (height), i.e., a square floor. The ceiling, floor, and vertical walls were assumed to be adiabatic. The left and right boundaries were fully open, modeled as pressure boundaries with zero-gauge pressure to represent a well-ventilated space, and backflow was considered. The inflow air temperature was 25 °C, and the relative humidity was 50%.

The second setting is about the two people in close distance (Figure 1), as various parameters affect inhalation- or spray-related short-range exposure. Chen et al. (2020) devised a steady-state analytical model to study inhalation and exhalation of two people with equal body height. The settings here are developed to be as close as possible to those in Chen et al. (2020).

In the present study, the *worst* situation in term of exposure was first modeled using two spheres (Scenario 1, which is also denoted the ideal scenario), each with a head diameter of 0.2 m. Both spheres were assumed to be adiabatic. Gravity was turned off to eliminate the buoyancy effect for air (the continuous phase), enabling the airflow exhaled by the source to develop horizontally to reach the target. However, the effect of gravity was considered for droplet tracking. These were largely similar to the settings studied by Chen et al. (2020); however, in the current study, no buoyancy was exerted on the expired jet, while Chen et al. (2020) considered the upward jet trajectory. Scenario 1 (spheres) eliminated the influences of height difference, and using this setting, we intended to obtain insights into the physical aspects. We also considered two human manikins standing face-to-face (Scenario 2), with consideration of body thermal

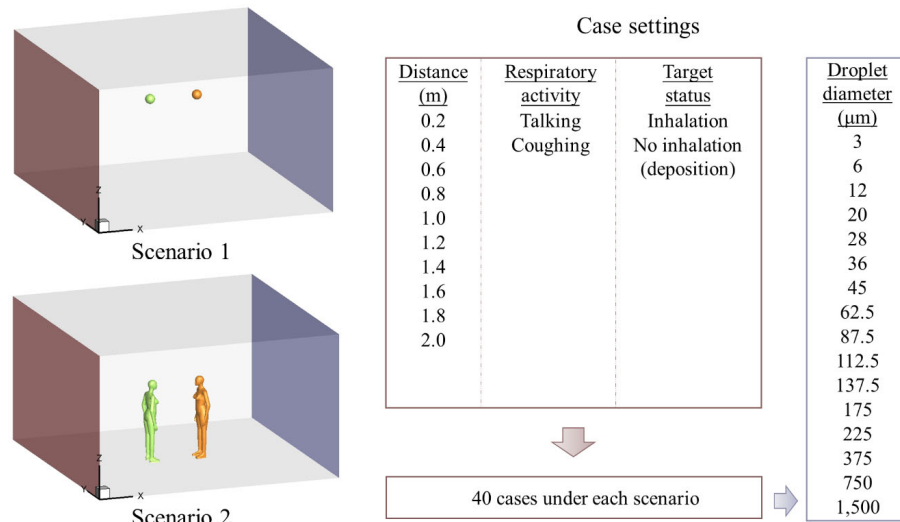


Fig. 1 Schematic of simulation scenarios and case settings. The source is colored orange, while the target is colored green. The left and right sides are pressure boundaries. A total of 80 cases are simulated with 40 cases for each scenario

convection boundary layers. Such convection boundary layers were generated because the body surface was warmer than the surrounding air environment. Scenario 2 (human manikins) was applied to test the applicability of the analytical model using real-human-shaped manikins. The height difference is not studied here, and the sphere scenario represents the worst exposure situation, but not for the studied manikin scenario, the expired jet curves upward due to thermal buoyancy.

Estimating the inhalation exposure of the target may seem to be simple, as it involves specifying a constant inhalation velocity (1 m/s). However, providing a consistent definition of large droplet deposition at mouth is not simple. When mouth is open, the deposition into oral cavity may be counted as inhalation, and those on lips are counted as large droplet deposition. The exact boundary between the two is a tricky question. In practice, the target may close mouth at some time. To distinguish between transmission caused by deposition on lip surfaces and that due to inhalation, we conducted a separate modeling study in which the mouth was closed and a wet area of the mouth membrane was specified, as in Chen et al. (2020) (Table 2). The non-inhale situation may present the “best” scenario for counting large droplet deposition.

Forty cases were simulated for each of Scenario 1 (spheres) and Scenario 2 (human manikins), to give a total of 80 cases. These included 10 distances (0.2–2.0 m with an increment of 0.2 m), talking and coughing situations, and an open-mouth situation for inhalation modeling and a closed-mouth for deposition modeling. The distance was defined as the distance between the mouths of the source and the target. The mouth outlet velocities of the source during talking and coughing actions were set as 3.9 and

11.7 m/s, respectively (Chao et al. 2009). The exhalation temperature was 35.1 °C (Popov et al. 2007), and the relative humidity was 100%.

Each of the 80 cases is denoted as Case [scenario (sphere or manikin), distance, source respiratory activity (talking or coughing), target model (inhalation or deposition)]. For example, Case [sphere, 1.0 m, talking, inhalation] represents the ideal (two sphere) scenario without buoyancy. The distance between the spheres was 1.0 m; the source action was talking, and the target action was active inhalation.

For each case, a range of droplets with initial sizes of 3 to 1,500 μm (as reported by Duguid (1946)) was tracked, although more recent studies have suggested different size distributions of expiratory droplets (e.g., Morawska et al. 2009; Somsen et al. 2020). Note that the use of “droplets” implies their ability to evaporate for the whole size range.

In the manikin scenario (Scenario 2), the manikin was from an earlier study by Liu et al. (2017). In the current study, a different segregation of body parts was implemented. The manikin height and total surface area were 1.69 m and 1.5 m², respectively. Only convective heat transfer was considered. Each manikin was segregated into the following body parts: head (excluding facial membranes), eye, nose, mouth, neck, chest, upper arm, forearm, pelvis, thigh, knee, lower leg, and feet (Figure 2). The body parts were divided such that different heat fluxes could be considered. Peripheral body parts such as feet and hands exhibited a high convective heat transfer coefficient, while the body center exhibited a low value (de Dear et al. 1997; Xu et al. 2019). The convective heat transfer coefficients for the body parts of a nude upright thermal manikin measured by de Dear et al. (1997) were used. The coefficients for body parts that were present in our study but absent in de Dear et al. (1997) were taken as

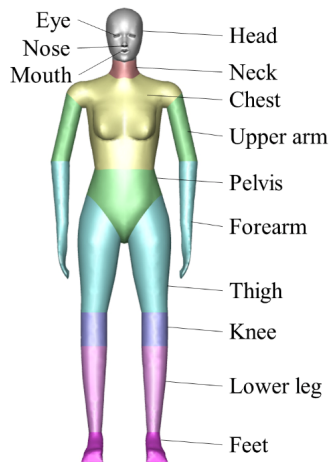


Fig. 2 Illustration of segregation of manikin body surface

the average value of adjacent body parts. For example, the coefficient for the neck was the average of those for the head and chest (see Table 1 for detailed information). The heat flux at each part was estimated according to the temperature difference. We assumed an ambient temperature of 25 °C and an average actual skin temperature of 31.8 °C (note that skin temperature can vary with environmental conditions), as measured on human volunteers (Craven and Settles 2006). de Dear et al. (1997) used a constant mean skin-to-air temperature gradient to calculate the heat transfer coefficient and did not report a body-part-specific temperature. In the current study, considering that the temperatures of body parts differ with environmental settings and ventilation modes, a single value was assumed for the temperature gradient, although the resultant body-segment-specific temperature was not a constant value.

2.2 Numerical methods

The simulation was conducted in ANSYS Fluent 18 (Pennsylvania, United States), and the governing equations were discretized via the finite volume method. A coupled algorithm was used for pressure-velocity coupling, and the gradient was computed via the Green-Gauss node-based method. Variables were discretized using the second-order upwind scheme. The Boussinesq assumption was adopted to incorporate the influence of the buoyancy-driven flows. The renormalization group k-epsilon model developed by Yakhot and Orszag (1986) with enhanced wall treatment was adopted, owing to its simulation accuracy and reasonable computational expense in indoor environments with thermal manikins (Gao and Niu 2005). The simulation was conducted with double precision. Convergence was considered to be reached when the residuals were less than 1×10^{-6} for energy and 1×10^{-3} for other quantities, and the monitored values remained stable for at least 2,000 iterations. The simulation was run on a Dell server R920. The mesh was generated in Ansys ICEM with prism layers surrounding the manikin surfaces ($y^+ < 5$). The results of the grid independence test are presented in Supplementary Material A, and a validation case of the flow field was presented in Supplementary Material B, which are available in the Electronic Supplementary Material (ESM) in the online version of this paper.

For each case, a steady flow field was first obtained and then particle tracking was performed using the converged steady flow field. As all simulations were conducted under steady-state conditions, no breathing function with time or synchronization between the source and the target was considered.

Table 1 Information on manikin body segregation and heat generation

	Body surface area (m ²)	Natural convective heat transfer coefficient (W·m ⁻² ·K ⁻¹)	Natural convective heat flux (W·m ⁻²)*	Natural convective heat transfer (W)
Head	0.0982	3.6	24.48	2.4039
Eye	0.0006	3.6	24.48	0.0147
Nose	0.0002	3.6	24.48	0.0049
Mouth	0.0003	3.6	24.48	0.0073
Neck	0.0185	3.275	22.27	0.4120
Chest	0.2950	2.95	20.06	5.9177
Upper arm	0.1154	2.9	19.72	2.2757
Forearm	0.1574	3.9	26.52	4.1742
Pelvis	0.1467	3.4	23.12	3.3917
Thigh	0.3287	4.1	27.88	9.1642
Knee	0.0778	4.1	27.88	2.1691
Lower leg	0.1668	4.1	27.88	4.6504
Feet	0.0940	5.1	34.68	3.2599
Sum	1.4996	—		37.8457

* Assumed temperature difference: 6.8 K.

2.3 Particle tracking

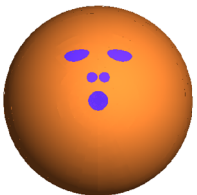
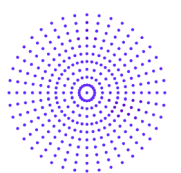
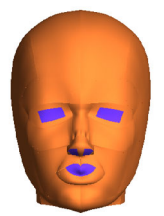
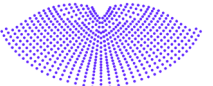
As mentioned, droplets with a wide range of initial sizes were tracked for each case. The governing equations for the discrete phase are summarized in Supplementary Material C, and the validation of the particle tracking algorithm is described in Supplementary Material D, in the online version of this paper. The expired droplets for our simulations were assumed to be water droplets with a density of 1000 kg/m³, and they are assumed to be capable of evaporating to a final diameter of 32.5% of their initial diameter by assigning a volatile fraction (Wei and Li 2015). The above treatment involves no explicit introduction of various components and only has a minimal effect considering that the majority component of droplets is water. Drag force and gravity were considered for droplet tracking while other forces including pressure gradient force, Magnus lift force, and Basset history force were ignored. The droplets were released from a file containing information on initial conditions (position, velocity, temperature, and diameter). The injected droplets were assumed to have the same temperature and injection velocity as the source respiratory activities. The droplet injection positions are shown in Table 2. The facial membrane areas were consistent with that in Chen et al. (2020) for comparison purposes; the surface areas of the two eyes and nostrils were 6 and 2 cm², respectively. In Scenario 1 (spheres), the mouth was a circle with a 2 cm diameter, and in Scenario 2 (human manikins), the surface area of the mouth was 3.14 cm².

Owing to the relatively small facial membrane area, a large number of trajectories were needed. For Scenario 1, 100 droplets were released from each of the 341 injection positions, and tracked at 0.2, 0.4, 0.6 and 0.8 m from the source (each injection position with 100 trajectories, and

34,100 trajectories in total) and 200 droplets for distances at 1–2 m with a step of 0.2 m (each injection position with 200 trajectories, and 68,200 trajectories in total). For Scenario 2, 50 droplets were released from each of the 600 injection positions and tracked for distances less than or equal to 0.4 m (30,000 trajectories in total) and 100 droplets for distances greater than or equal to 0.6 m (up to 2 m, 60,000 trajectories). The discrete phase model (DPM) boundary condition for the target mouth was set as “escape” for active inhalation and “trap” for passive deposition. Droplets were assumed to be trapped on other body parts, including eyes and nostrils. The “reflect” boundary condition was applied to the room ceiling; the “trap” boundary condition was applied to the vertical walls and floor; and the “escape” boundary condition was applied to the pressure boundaries on the left and right sides (Figure 1). The average residence time of the “incomplete” droplets (those that remained suspended in the computation region without a final fate) was considered as a proxy for the average time of the system.

A constant step length factor of 5 was used, and the number of steps for particle tracking was increased until stable and reliable results were obtained. The following two criteria were considered. (1) The residence time of droplets suspended in the computation region was sufficiently longer than the time required for the droplets to reach the target. For instance, it takes less than or equal to 0.5 s for 3 μm droplets released from the mouth to reach a target face 0.4 m away under talking conditions. Each droplet is tracked for sufficiently long time and at the end of simulation, less than 10% of the droplets remain the computational domain. (2) The number of droplets inhaled through the target mouth (the short-range inhalation route), the number of droplets deposited on the target mouth, noses, and eyes

Table 2 The defined facial membranes shown in purple for the target and droplet injection positions of source’s mouth in Scenarios 1 (spheres) and 2 (human manikins)

Scenario	Facial membranes shown in purple	Injection positions at mouth	Number of injection positions
Two spheres			341
Two human manikins			600

(the large droplet route), and the number of droplets deposited on the target head via both routes remained constant because the head region was particularly important in the exposure investigation. We assumed that the effects of droplets on the continuous phase were minimal, and the numerous trajectories were only for statistical analysis; thus, the one-way coupling rule was adopted.

3 Results

3.1 Airflows interacting between two spheres or two manikins

Droplet transport, dispersion, and deposition occur in the

airflow field. As we considered a steady-state setting, the airflow fields were first obtained for each of the 80 cases. The temperature contours in Scenario 2 (human manikins) for talking and coughing at several distances are shown in Figures 3 and 4, respectively. For talking, the positive buoyancy drives the exhaled air from the source upward. This buoyancy effect impacts less on the expired flow within 0.6 m so that the target is still vulnerable in term of exposure. Beyond 0.6 m, small droplets follow the upward airflows, hence bypass the target head, while larger droplets follow their own momentum, and may be inhaled by the target or deposit on the target's head (Figure 3). This observation may only be applicable in the special setting considered. The buoyancy effect becomes minimal in the

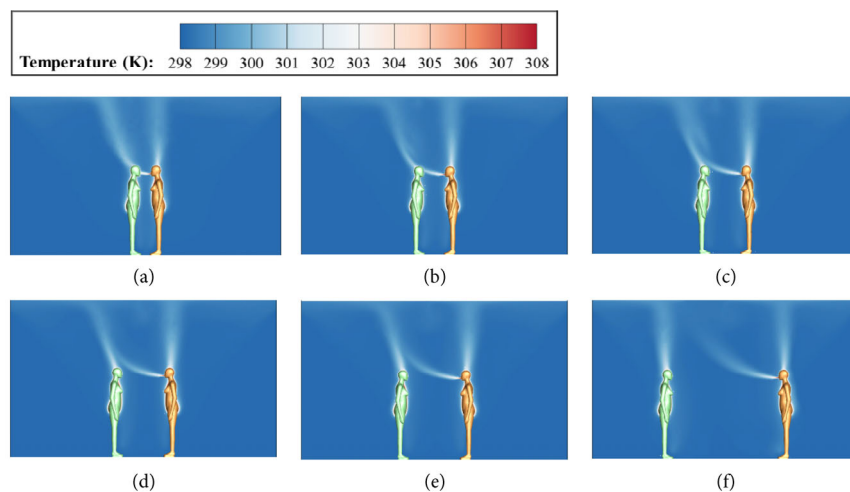


Fig. 3 Air temperature distribution mid-plane in the room in Scenario 2 (human manikins) at six distances (0.2–2.0 m) in cases in which the source talked and the target manikin did not inhale: (a) Case [manikin, 0.2 m, talking, deposition]; (b) Case [manikin, 0.4 m, talking, deposition]; (c) Case [manikin, 0.6 m, talking, deposition]; (d) Case [manikin, 0.8 m, talking, deposition]; (e) Case [manikin, 1 m, talking, deposition]; (f) Case [manikin, 2 m, talking, deposition]

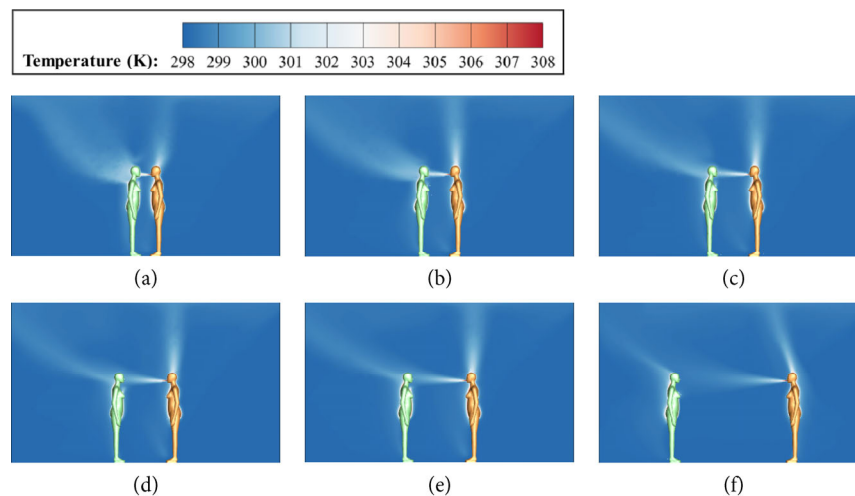


Fig. 4 Air temperature distribution mid-plane in the room for Scenario 2 (human manikins) at six distances (0.2–2.0 m) in cases in which the source manikin coughed and the target manikin did not inhale: (a) Case [manikin, 0.2 m, coughing, deposition]; (b) Case [manikin, 0.4 m, coughing, deposition]; (c) Case [manikin, 0.6 m, coughing, deposition]; (d) Case [manikin, 0.8 m, coughing, deposition]; (e) Case [manikin, 1 m, coughing, deposition]; (f) Case [manikin, 2 m, coughing, deposition]

case of coughing due to its high velocity (Figure 4). A greater exhalation velocity means a greater momentum relative to the buoyancy effect. In the case of coughing, the target is affected even at 2 m away from the source. Thus, coughing increases the infection risk at a close range. The relative humidity contour figures are similar to the temperature contours (Supplementary Material E). It was assumed that no water vapor was generated at the body surface, resulting in lower relative humidity around the manikins and within the thermal plume owing to a relatively higher temperature, while the ambient relative humidity was $\sim 50\%$.

The velocity contours in Scenario 1 (spheres) for talking are shown in Supplementary Material E. The streamlines for Scenario 1 (spheres) are revealed in Figure 5. Figure 5(a) shows the case in which airflow surrounds the target head, and Figures 5(b) and (c) show magnified views of the streamlines with target deposition and inhalation, respectively. For deposition, a stagnation point occurs at the target mouth, and for inhalation, the streamlines first diverge in front of the target mouth and then converge when entering the orifice. This “anisokinetic aerosol sampling” process with a spherical sampler was theoretically modeled by Dunnett and Ingham (1988) and was used for analytical exposure analysis by Chen et al. (2020).

3.2 Change in droplet characteristics

The transport of exhaled droplets can be predicted using the steady-state flow fields obtained in Section 3.1. The changes in the diameter, temperature, and velocity of droplets with different initial diameters differed with source–target distance and respiratory activity (talking and coughing; Figures 6, Figure 7). Here, we only report the data for Scenario 1 (spheres) at a distance of 2 m. The droplet information was recorded every 0.1 m. Figures 6 and 7 were constructed using the trajectory data of 40 droplets instead

of all tracked droplets (otherwise, an incredibly large droplet history file would have been generated). This explains the fluctuations present in Figures 6 and 7, particularly for the smaller droplets, as they were more influenced by turbulence than the larger droplets.

Droplet diameters were normalized according to their initial exhalation size in Figures 6(a) and 7(a). As some droplets may not be able to travel 2 m, parameters were drawn only within the maximum range that they could reach. Overall, droplet behaviors agree well with those presented in Chen et al. (2020). During both talking and coughing, droplets smaller than $100\ \mu\text{m}$ were most likely to evaporate to their final size before travelling 2 m, although a faster evaporation rate occurred during talking because of its smaller injection velocity and longer suspension in air. The smaller the droplet size, the faster the evaporation. For droplets larger than $100\ \mu\text{m}$, there was either no change or a very small change in diameter within the observation distance. Droplets of $\sim 100\text{--}400\ \mu\text{m}$ were mainly controlled by gravity and could not travel far. Larger droplets ($>400\ \mu\text{m}$) were mainly inertia-driven. Gravity was insufficient to change the initial horizontal movements of the droplets. However, a very short relaxation time for small droplets ($<50\ \mu\text{m}$) caused their velocity magnitude to rapidly decrease.

The temperature changes depicted in Figures 6(b) and 7(b) also confirm the above pattern; that is, the temperatures of small droplets converged to the room temperature of $298.15\ \text{K}$ ($25\ ^\circ\text{C}$) after full evaporation. A continuous decrease in temperature indicated unfinished evaporation, which can be observed for droplets larger than $100\ \mu\text{m}$.

Through CFD modeling, Zhu et al. (2006) and Sun and Ji (2007) have also observed the above changes in droplet behaviors. According to the differences in the changes in droplet behaviors, three categories of droplet diameter ranges were defined: less than $50\ \mu\text{m}$, $50\text{--}100\ \mu\text{m}$, and greater than $100\ \mu\text{m}$.

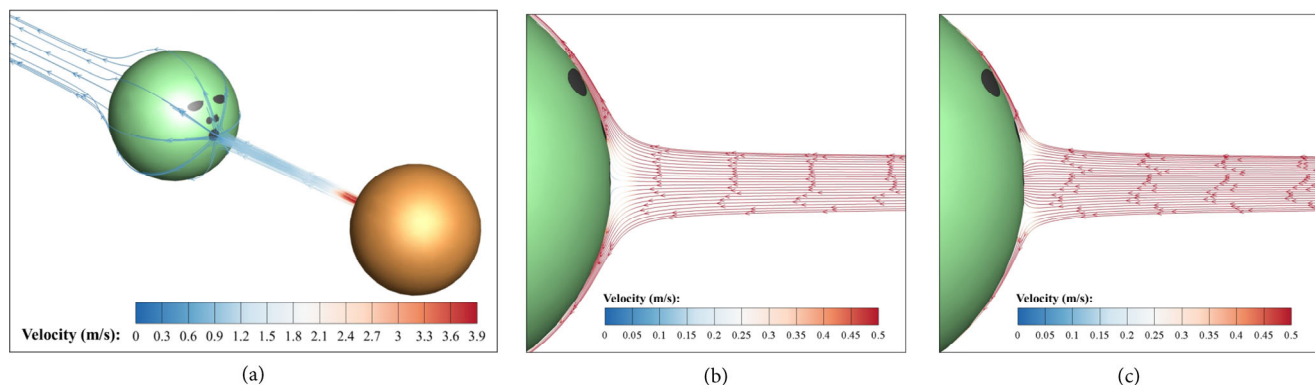


Fig. 5 (a) 3D streamlines for Case [sphere, 0.4 m, talking, deposition]; (b) magnified views of 2D streamlines near the target mouth for Case [sphere, 0.4 m, talking, deposition]; and (c) magnified views of 2D streamlines near the target mouth for Case [sphere, 0.4 m, talking, inhalation]. The different airflow pattern between (b) and (c) is caused by a lack of inhalation in (b) and with inhalation in (c)

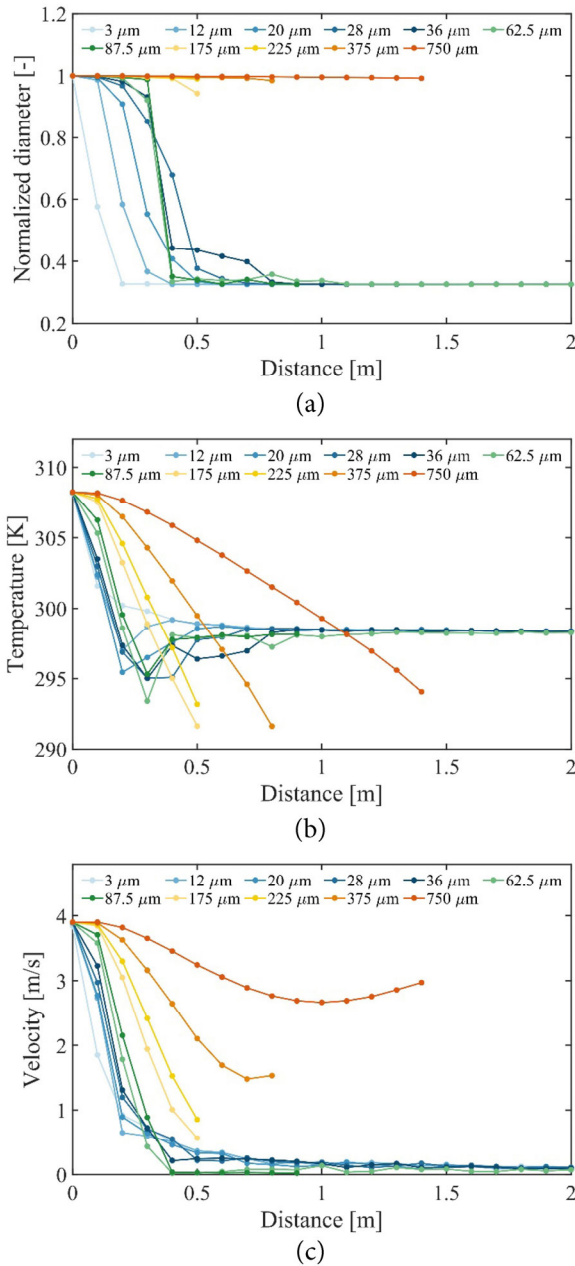


Fig. 6 Changes in the (a) normalized diameter, (b) temperature, and (c) velocity magnitude of droplets with different initial diameters as a function of distance for Case [sphere, 2 m, talking, deposition]

Figures 8 and 9 intuitively depict the droplet trajectories for Scenario 2 (human manikins) during talking and coughing, respectively. Forty trajectories with a distance of 0.6 m are shown. These trajectories originated from a *single* release point in the middle of the source mouth. During talking, droplets with diameters of 36 and 62.5 μm followed the buoyancy-driven upward flow; however, gravity began to increase its effect on the 62.5 μm droplets, so that droplets with a diameter of greater than or equal to 62.5 μm exhibited a downward trend. A significant difference existed between

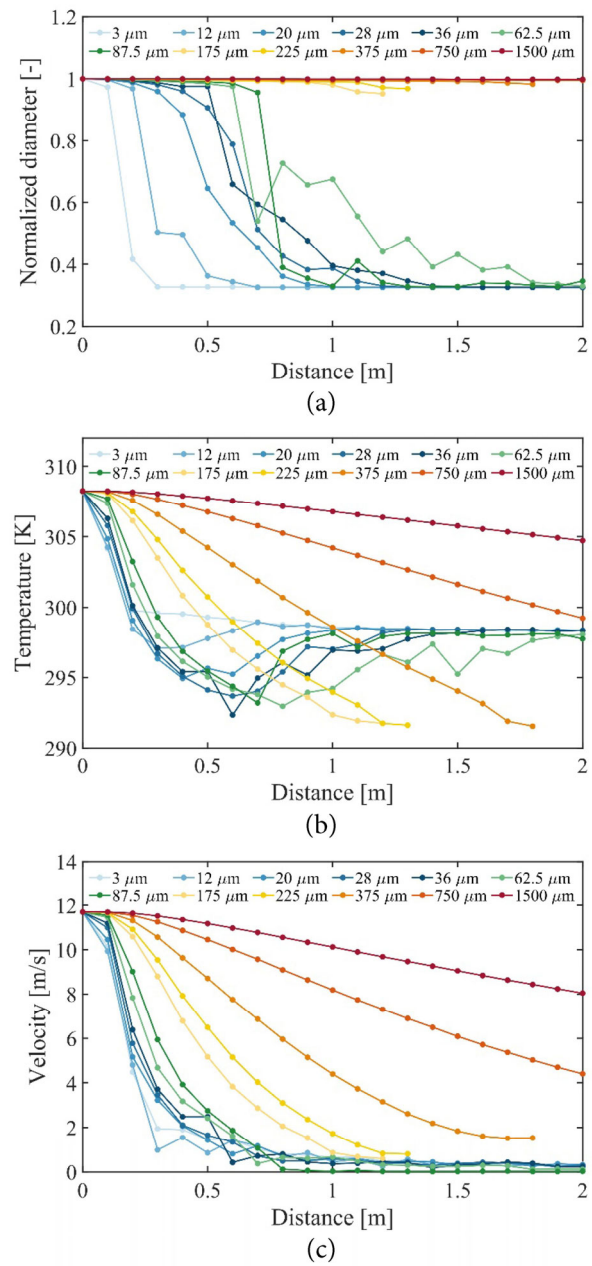


Fig. 7 Changes in the (a) normalized diameter, (b) temperature, and (c) velocity magnitude of droplets with different initial diameters as a function of distance for Case [sphere, 2 m, coughing, deposition]

the 87.5 and 112.5 μm droplets: the former remained able to move upward, while the latter largely fell onto the floor. During coughing, droplets of all sizes showed more consistency; they moved forward almost horizontally with greater initial momentum than during other actions. For both talking and coughing, the effect of turbulence on droplets smaller than 100 μm was significant, but droplets greater than 100 μm in size were barely influenced by buoyancy or turbulence, and their trajectories were more consistent than those of droplets less than 100 μm in size. Droplet

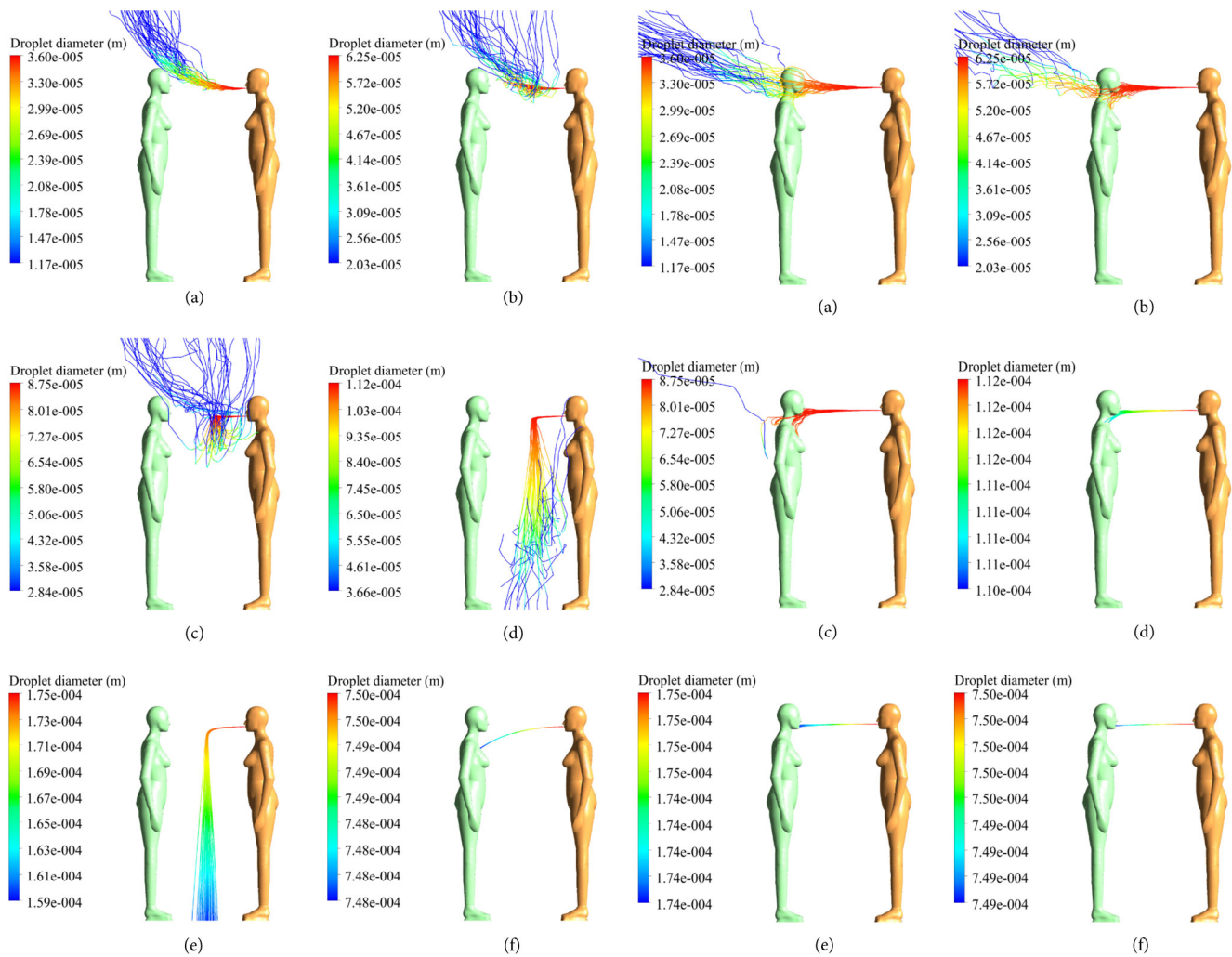


Fig. 8 Trajectories of droplets with an initial diameter of (a) 36 μm , (b) 62.5 μm , (c) 87.5 μm , (d) 112.5 μm , (e) 175 μm , and (f) 750 μm for Case [manikin, 0.6 m, talking, deposition] (trajectories are colored by diameter)

Fig. 9 Trajectories of droplets with an initial diameter of (a) 36 μm , (b) 62.5 μm , (c) 87.5 μm , (d) 112.5 μm , (e) 175 μm , and (f) 750 μm for Case [manikin, 0.6 m, coughing, deposition] (trajectories are colored by diameter)

characteristics with different sizes shown in Figures 6–9 also rationalize the necessity for considering a wide range of diameters.

3.3 Estimated exposure on facial membranes

Facial membranes such as eyes, nostrils, and mouth are directly exposed to incoming droplets. We used the estimated exposure on the facial membranes as defined in Table 2 as a measure of large droplet transmission. Virus-laden droplets could either passively deposit on membranes (i.e., the large droplet route) or be inhaled through active breathing (i.e., the airborne or inhalation route). Deposition and inhalation were considered as independent processes. For deposition, all facial membranes (eyes, nostrils, and the mouth) were involved, and inhalation was absent. For inhalation, we assumed mouth inhalation only.

We defined a new parameter—the number ratio—as the ratio of the number of droplets inhaled by the target or deposited on the target membranes to the total number of droplets released at the source mouth. The change in the number ratio as a function of distance is depicted in Figures 10 and 11 for Scenarios 1 (spheres) and 2 (human manikins), respectively. Each figure contains two plots, for droplets with diameters of less than or equal to 87.5 μm and greater than or equal to 87.5 μm . Scenario 1 (spheres) produced the highest possible exposure, as the exhaled air stream reached the front of the target. In Scenario 2 (human manikins), the buoyancy effect drove the exhaled airflow upward, leading to relatively smaller exposure values compared with Scenario 1 (spheres). In both scenarios, a rapid decay in the number ratio (for either inhalation or deposition) occurred during talking. During talking, there was a dramatic decrease in exposure for droplets smaller

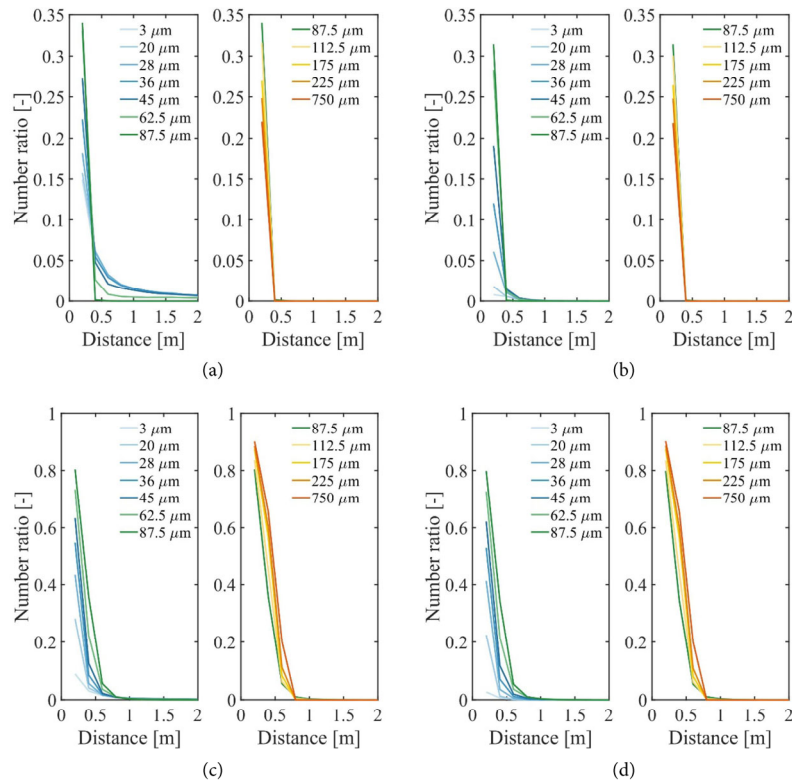


Fig. 10 Changes in the number ratio of facial membrane exposure as a function of distance: (a) Case [sphere, 0.2–2 m, talking, inhalation]; (b) Case [sphere, 0.2–2 m, talking, deposition]; (c) Case [sphere, 0.2–2 m, coughing, inhalation]; (d) Case [sphere, 0.2–2 m, coughing, deposition]

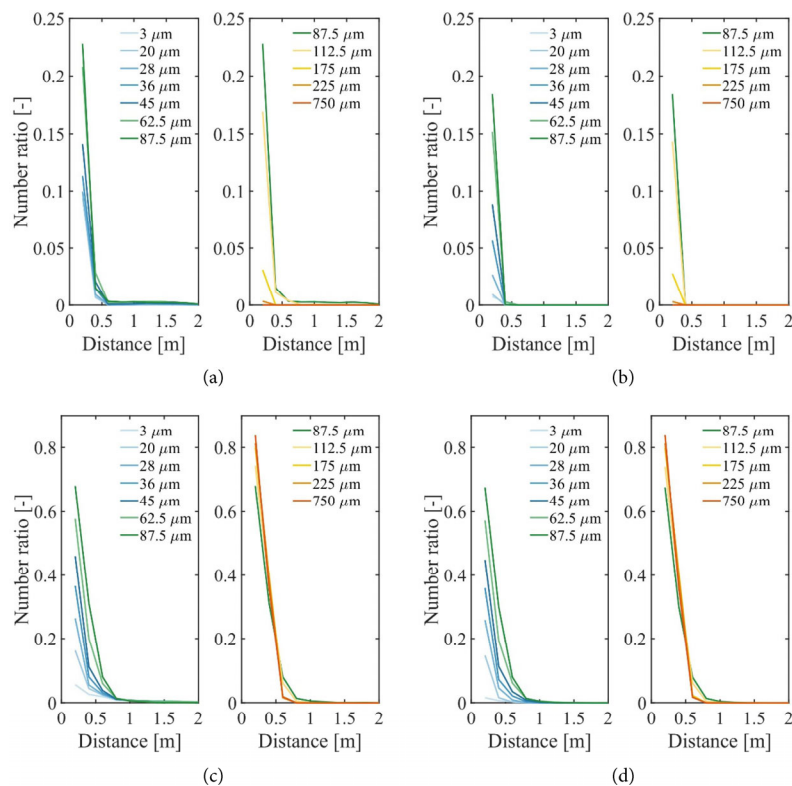


Fig. 11 Changes in the number ratio of facial membrane exposure as a function of distance: (a) Case [manikin, 0.2–2 m, talking, inhalation]; (b) Case [manikin, 0.2–2 m, talking, deposition]; (c) Case [manikin, 0.2–2 m, coughing, inhalation]; (d) Case [manikin, 0.2–2 m, coughing, deposition].

than $50\ \mu\text{m}$ due to deposition than inhalation. The small droplets followed the airflow and bypassed the target more easily than the larger droplets. During talking and within $0.4\ \text{m}$, droplet exposure increased with droplet diameter for those droplets with diameters less than $87.5\ \mu\text{m}$ and decreased for those droplets with diameters larger than $87.5\ \mu\text{m}$. The ability of droplets to follow the airflow and the effect of gravity led to the peak exposure being to droplets with a diameter of $87.5\ \mu\text{m}$. This cutoff diameter was not observed for coughing-related droplets, as exposure consistently increased with droplet size within $0.4\ \text{m}$. This can be explained by the movements of droplets with different momentums, as shown in Figures 8 and 9. In both scenarios, inhalation resulted in a greater exposure than deposition during talking, while both figures show there was no significant difference between inhalation and deposition during coughing. The dominance of the short-range airborne route over the large droplet route was significant at greater distances.

3.4 Ratio of the large droplet route to the short-range inhalation route (LS exposure ratio)

The LS exposure ratio (i.e., the ratio of volumetric exposure due to deposition to volumetric exposure due to inhalation) was defined by Chen et al. (2020) and compares the relative importance of deposition (large droplet exposure) and inhalation (short-range airborne route) during short-range exposure. An LS ratio of unity means that exposure due to

short-range inhalation is equal to that due to large droplet deposition.

Figure 12 summarizes the estimated LS exposure ratios in this study and the analytical results reported by Chen et al. (2020). Scenario 1 (spheres) featured more deposition than Scenario 2 (human manikins) at large distances, while no significant differences existed between the scenarios at small source–target distances. The CFD results of both scenarios agree well with the analytical results for the overall droplet size range (Figure 12(d)), while the analytical results underestimated the deposition of small- and medium-sized droplets from both talking and coughing. The inconsistency is attributable to the oversimplicity of the analytical model.

Chen et al. (2020) adopted the velocity at the front of the target mouth as the incoming airflow velocity to calculate the required Stokes number. In contrast, in the present study, the velocity at a single point was an underestimation of the incoming airflow velocity, as it should be higher than the value at the point considering the continuous velocity decay from the source mouth to the target mouth. A lower velocity value led to greater inhalation-related exposure and lower deposition-related exposure. This was one of the shortcomings of theoretical analysis; it was difficult to ascertain which velocity value to use, and any other point did not necessarily provide a better prediction or sounder logic.

CFD simulations confirmed the dominance of short-range inhalation as seen in the analytical model. First, both

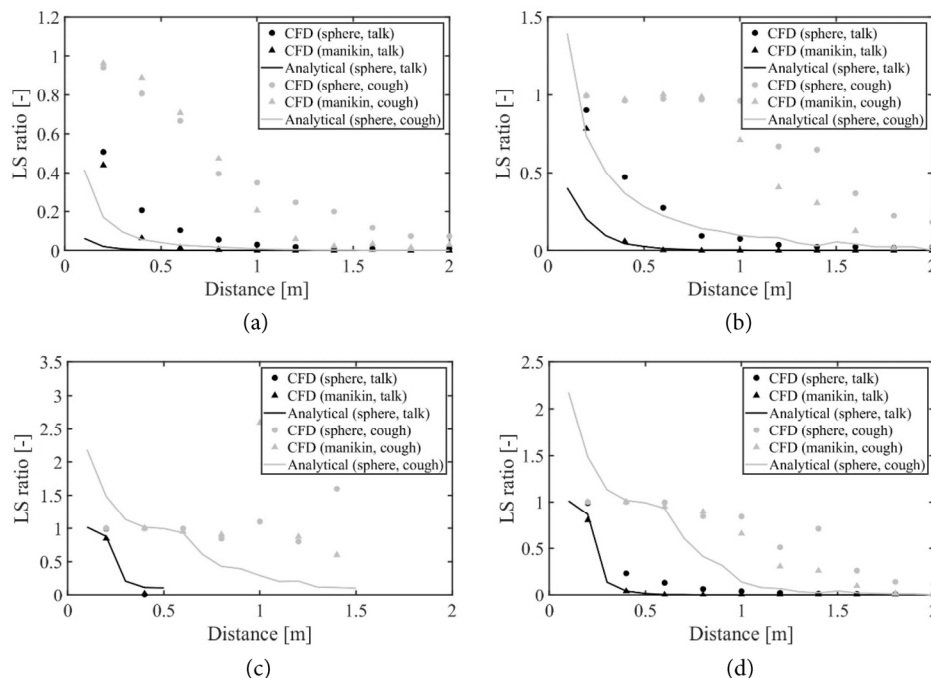


Fig. 12 LS exposure ratio (the ratio of the large droplet route to the short-range inhalation route) in Scenarios 1 (spheres) and 2 (human manikins) for droplets with an initial diameter of (a) less than $50\ \mu\text{m}$, (b) $50\text{--}100\ \mu\text{m}$, (c) greater than $100\ \mu\text{m}$, and (d) the overall range. The analytical results are from Chen et al. (2020)

methods showed that droplets smaller than $50\ \mu\text{m}$ were most closely related to airborne transmission (Duguid 1946; Morawska et al. 2009; Lindsley et al. 2010; Somsen et al. 2020). The *LS* exposure ratios for all investigated distances were less than 1 for coughing, and even less for talking, which indicates that the short-range inhalation route dominated exposure in short-range transmission. Second, a plateau region in which the large droplet sub-route and the airborne sub-route were equally important for coughing was predicted. According to the new CFD results, this region appeared in the medium-size range ($50\text{--}100\ \mu\text{m}$) and the larger range ($>100\ \mu\text{m}$). Third, the *LS* ratios in Scenario 2 (human manikins) (Figure 12(d)) showed the best consistency with the analytical results, and the region of the large droplet-route dominance ($\sim 0.2\ \text{m}$ for talking and $0.6\ \text{m}$ for coughing) approximately coincides with that in Chen et al. (2020), although during coughing, a slower decay occurred beyond the first $0.6\ \text{m}$.

3.5 Deposition on head

The surface of the target head contained two parts: the facial membranes and other parts. Here, we present the results for the number of deposited droplets on the non-facial-membrane surface of the head. There is the possibility of infection when a person touches their face and then touch their nasal or oral membranes. Considering the high frequency of self-touching and the insufficient time for virus deactivation, the infection risk associated with self-touching can be significant. The self-touching route is denoted the immediate surface route (Zhang et al. 2020a).

The facial membrane area and head size vary among people. The total head surface area (excluding the eyes, nostrils, and mouth) for Scenario 2 (human manikins) was $0.0982\ \text{m}^2$. The number ratios of deposited droplets on the target head (excluding facial membranes) are shown in

Figure 13. Only results for Scenario 2 (human manikins) were shown here since it represented real-human-shaped deposition and made more practical sense.

Generally, the effect of active inhalation or non-inhalation (i.e., inhalation and deposition) on the target head exposure was minimal during both talking and coughing. Therefore, the results shown here are only for deposition. Under the two respiratory activities, droplets smaller than $50\ \mu\text{m}$ showed a pattern of decreased exposure with distance and increased exposure with diameter.

In contrast, a peak exposure value appeared for coughing-induced droplets larger than $50\ \mu\text{m}$, with the value increasing and appearing at a greater distance as droplet size increased. At very short range, large coughing-induced droplets were exhaled and moved forward almost horizontally, leading to a high “mouth-to-mouth” exposure; as distance increased, the trajectories bent downward and more droplets missed the target mouth and deposited on the target head, leading to a peak value as in Figures 13(b). Different from the head, the limited surface areas and specific locations of facial membranes led to an absence of the peak value for droplets larger than $50\ \mu\text{m}$ during coughing (Figures 10 and 11). The cutoff size of $87.5\ \mu\text{m}$ for facial membrane exposure during talking did not apply to head exposure. As the two mouths were at the same height, the $87.5\ \mu\text{m}$ droplets were largest droplets that were able to move forward without falling, while droplets larger than $100\ \mu\text{m}$ tended to miss the target mouth but nevertheless impacted the chin.

The greater inertia carried by larger droplets dramatically increased exposure risk, although these droplets were quite rare. Compared with facial membrane exposure in Scenario 2 (human manikins) (Figure 11), a prominent increase in the exposure number ratio and an extended affected distance occurred, implying a risk of exposure through the immediate surface route.

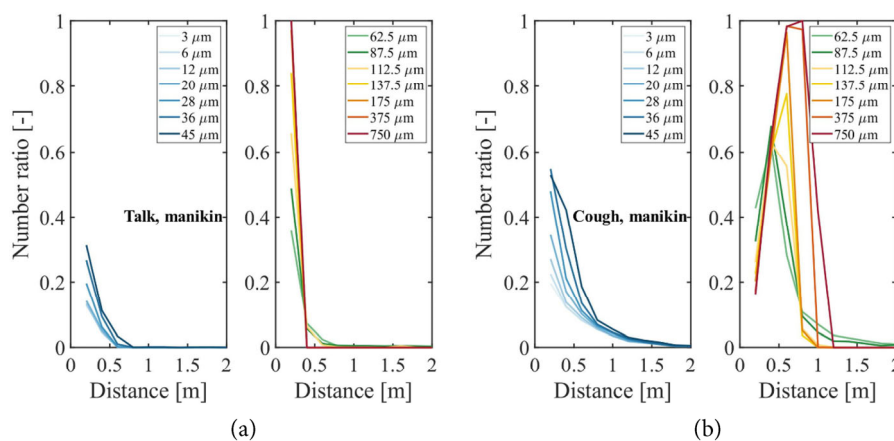


Fig. 13 Number ratio of the target head exposure due to deposition: (a) Case [manikin, 0.2–2 m, talking, deposition]; and (b) Case [manikin, 0.2–2 m, coughing, deposition]

4 Discussion

4.1 Confirmation of the dominance of the short-range inhalation route via CFD simulations

The CFD modeling of two simple settings confirmed the analytically derived predominance of the short-range inhalation route over large droplet transmission between two people at short range. The following two major assumptions in the original analytical model (Chen et al. 2020) are verified by the new CFD simulations, i.e., the human head was a sphere so that deposition of particles can be estimated using the literature data, and the “anisokinetic aerosol sampling” approximates the inhalation. Exhaled droplets smaller than 50 μm have been commonly identified (Duguid 1946; Morawska et al. 2009; Lindsley et al. 2010; Somsen et al. 2020), and the CFD results confirmed that even for coughing, short-range inhalation was more important than the large droplet route at a very close distance (0.2 m) for exhaled droplets less than 50 μm in size. Although nasal breathing was not considered in this study, it is reasonable to infer that inhalation route would also dominate given the small dispersed expiratory velocity. Such droplets were able to quickly evaporate to their final size, and the resulting nuclei exhibited a strong ability to follow airflow owing to their small Stokes number. When the droplet-laden airflow approached the blunt head of a quiescent target without active inhalation, the small droplets followed the airflow and bypassed the target. This explains why the deposition of such small droplets was rare. When a target was actively inhaling, the inhalation velocity was generally greater than the incoming air velocity, which led to “super-isokinetic aerosol sampling.” Airflow converged and entered the orifice (Figure 5(c)), and these small droplet nuclei followed the inhaled airflow. Given the rarity or low probability of deposition on facial membranes, this explains why the short-range airborne route dominated for small droplets in an environment with relatively low ambient velocity.

Separate simulations were conducted for inhalation and deposition. For the simulation of inhalation, the mouth was open. For the simulation of facial deposition, the mouth was closed, and all facial membranes (eyes, nostrils, mouth) were involved in the deposition. It is reasonable to infer that in the real world in which these two processes occur simultaneously, deposition exposure will be smaller; that is, the large droplet exposure in our study is likely an overestimation.

A unity LS ratio does not mean there was an equal infection *risk* for the two sub-routes. Inhaled droplets/particles have a greater probability of eventual deposition in the respiratory tract and thus causing infection, while droplets

deposited on facial membranes must undergo further indirect processes for eventual deposition in the respiratory tract. Droplets deposited on these facial membranes have been suspected to remain infectious for a long time; however, the exact mechanisms are unknown. Regarding the exterior membrane of the mouth, lip pursing may lead to further droplet movement, and the eyes are suspected to be an entry point for droplets (Coroneo and Collignon 2021). Self-hand-touching is another potential route. Thus, a value greater than 1 means that the large droplet route *possibly* dominates, while a value less than 1 means that the short-range inhalation route dominates. Thus, only a very large LS ratio ($\gg 1$) can lead to a predominant droplet route. Our estimated LS ratios are all less than 3.

The predominance of short-range airborne transmission over large droplet transmission has significant implications for intervention. First, mask wearing will work under limited transmissivity, such as during the early phases of a pandemic. Given the ongoing COVID-19 pandemic, wearing a facial mask has become a daily routine in numerous countries. Nevertheless, the recent new SARS-CoV-2 variant, Omicron, shows 160%–210% higher transmission rates compared than the Delta variant (Abbott et al. 2022) and has resulted in new waves of infection since December 2021. Normal surgical masks may not be sufficient in preventing transmission of Omicron. Therefore, it is recommended that people wear N95 masks when needed, particularly those exposed to higher infection risks such as health care workers. For long-range airborne transmission (which is beyond the scope of this study), improved space ventilation is recommended to mitigate risk (Li et al. 2007; Morawska et al. 2020) by decreasing droplet nuclei concentrations. Increasing ventilation above a certain threshold is found to be of diminishing effect (Chen et al. 2022; Jia et al. 2022). Provision of sufficient indoor space per occupant reduces the occurrence frequency of close contacts. Second, face shields, an intervention method to prevent large droplet transmission, may not be sufficient for mitigating respiratory infection.

4.2 Estimated critical droplet size related to the inhalation route: 87.5 μm

Our CFD study showed that a droplet size of 87.5 μm differentiates droplet behaviors. This critical size was also a cutoff determining whether full evaporation could occur before the droplets fell to the ground. Droplets of 60–100 μm fully evaporate before reaching 2 m, as shown in Xie et al. (2007) by revisiting the Wells evaporation-falling curve (Wells 1934). The cutoff size was influenced by expiratory velocity as well as ambient relative humidity. It is known that

the inhalable aerosols are smaller than 100–200 μm (Milton 2020). During talking (exhalation at 3.9 m/s), the 87.5 μm droplets could not reach 1 m, while during coughing (exhalation at 11.7 m/s), the droplets traveled as far as 2 m. The tracked droplet size was not continuous. We can only infer that under the conditions of this study, the critical size was approximately 87.5 μm .

A critical size of ~ 100 μm indicated that the size of droplets capable of being transmitted through an airborne route is much larger than the traditionally assumed droplet sizes (5 or 10 μm). Droplets larger than the critical size deposited at short ranges, whether on the floor or on the body surface of the target. Droplets smaller than 87.5 μm were the most frequently observed, implying that the airborne route dominated infection transmission. The commonly believed threshold size for airborne droplets (5 μm) was recognized to be misleading and was corrected during the COVID-19 pandemic (Prather et al. 2020). On the other hand, even though the inhalable droplet size was found to be ~ 100 μm , the size 5 μm is still important since it is the cutoff size that can reach the alveolar region (Milton 2020) and may potentially lead to more severe consequences than those deposited on the upper respiratory tract.

4.3 Risks associated with the short-range surface touching route

The surface touching route is important for enteric infection; however, the role of the surface touching route in the transmission of SARS-CoV-2 has been regarded as insignificant by the US Center for Disease Control. Zhang et al. (2021) reported a lack of long-range surface-touching transmission in a restaurant outbreak of COVID-19 in early 2020 in Guangzhou, China. Considering that the large droplet route, involving deposition on facial membranes, plays an in-negligible role, there is the possibility that the immediate surface route also plays an in-negligible role.

Deposition on the head of a target with the same height as the source could be significant, as demonstrated in this study. The total front face area was approximately 50 times that of facial membranes, and the total deposition on the face could reach 50 times that on the facial membranes. Compared with facial membranes, the head can be considered a much larger “deposited droplet receptor.” Through video analysis, Zhang et al. (2020b) found that people touched their mucous membranes an average of 34.3 times per hour and the middle region of their face (nose and mouth region) at a particularly high frequency. The authors also found that after volunteers touched their left/right cheeks, they also had a relatively high probability of touching the middle parts of their faces, particularly their lips or chin.

Considering that the deposition time can be short between two self-touches, the deposited viruses may retain good survivability. The virus transfer rate is affected by factors such as roughness, wetness, surface material, and force (Zhao et al. 2019). A rubbing action between the face and hand leaves approximately 50% of droplet nuclei on each surface at equilibrium (Zhao et al. 2018). With all of these factors considered, the probability of infection due to the immediate surface route cannot be ruled out.

Hand hygiene and surface hygiene need to be considered when examining long-range surface-touching transmission. Following Lei et al. (2020), hand hygiene and surface cleaning should be paired. In the immediate surface-touching route, the self-touching frequency is so high that it is unlikely that people will wash their hands as frequently as would be required. Moreover, even if people wash their hands very frequently, it is unlikely that they will rinse their faces very frequently. Thus, for people with a contaminated facial skin surface, washing only their hands and subsequently touching their face and then their mucous membranes presents a possible transmission mechanism. However, more detailed analysis is needed, and exposure to the immediate surface route over a short range must be quantified (with the aid of the number of droplets deposited on immediate surfaces, touching frequencies, droplet transfer rate, etc.) and its relative contribution compared with that of short-range airborne and large droplet routes.

4.4 Limitations of this study

First, only two scenarios were considered under specific settings owing to our limited computational power. The two scenarios generated 80 individual CFD simulations. Several other major factors were not evaluated, including ambient environmental factors and individual factors. The ambient factors include the effect of background airflows (ventilation rate and air distribution), air temperature and humidity, and room geometry (the location of an individual near a wall or corner may introduce complex interactions of airflows). Individual factors include height variation, nasal breathing (particularly important for low activity individuals), clothing (which affects body plumes), posture and gesture (sitting and lying differs from standing), hairstyles (which affect facial deposition both as a deposition site and as they alter airflows), head size, and facial membrane size (eyes, nostrils, and mouth size). However, we have probably considered the worst condition—two upright individuals facing each other (i.e., the setting with the greatest deposition)—meaning that our conclusions, in particular the predominance of short-range airborne transmission, likely have some general applicability. The computational

power also places restriction on simulating even smaller droplets down to $<1 \mu\text{m}$ if the particle tracking method is used. Second, only steady-state conditions were considered. Such approximations may apply at farther distances since the “train of puffs” in realistic conversations can produce a jet-like flow (Abkarian et al. 2020), but the application may be limited at very close range. A transient simulation with breathing functions and synchronization between a source and a target will generate more realistic results. Our steady state simulations served well the purpose of confirming the existing findings from an analytical model. Finally, large eddy simulations may be more suitable for achieving transient simulations than our approach, and many studies have focused on simulations of exhaled airflows (Abkarian et al. 2020; Behera et al. 2021). However, our adopted approach has enabled us to produce some useful results within the limits of our computational power.

5 Conclusions

Through CFD simulations, this study investigated exposure to inhaled and deposited droplets between a source and target separated by 2 m. We confirmed the findings of an early analytical study, i.e., that short-range inhalation dominates exposure at distances greater than or equal to 0.2 m for droplets smaller than $50 \mu\text{m}$ during talking and coughing, and the results for the overall droplet size range agree well with an early analytical model study. A critical droplet size of $87.5 \mu\text{m}$ was found to differentiate droplet behaviors. Coughing led to much greater exposure than talking, and the large droplet (deposition or spray) route grew more important with increasing exhalation velocity. The number of droplets deposited on the target head was much greater than the number deposited on mucous membranes, particularly during talking, indicating a risk of exposure through the immediate surface route at a short range.

Electronic Supplementary Material (ESM): the Supplementary Materials are available in the online version of this article at <https://doi.org/10.1007/s12273-022-0968-y>.

Acknowledgements

This work was supported by a General Research Fund (grant number 17202719) provided by the Research Grants Council of Hong Kong.

Declaration of competing interest

The authors declare that they have no known competing financial interests or personal relationships that could appear to influence the work reported in this paper.

References

- Abbott S, Sherratt K, Gerstung M, et al. (2022). Estimation of the test to test distribution as a proxy for generation interval distribution for the Omicron variant in England. medRxiv 2022.01.08.22268920.
- Abkarian M, Mendez S, Xue N, et al. (2020). Speech can produce jet-like transport relevant to asymptomatic spreading of virus. *Proceedings of the National Academy of Sciences of the United States of America*, 117: 25237–25245.
- Banik RK, Ulrich A (2020). Evidence of short-range aerosol transmission of SARS-CoV-2 and call for universal airborne precautions for anesthesiologists during the COVID-19 pandemic. *Anesthesia and Analgesia*, 131: e102–e104.
- Behera S, Bhardwaj R, Agrawal A (2021). Effect of co-flow on fluid dynamics of a cough jet with implications in spread of COVID-19. *Physics of Fluids*, 33: 101701.
- Chao CYH, Wan MP, Morawska L, et al. (2009). Characterization of expiration air jets and droplet size distributions immediately at the mouth opening. *Journal of Aerosol Science*, 40: 122–133.
- Chen W, Zhang N, Wei J, et al. (2020). Short-range airborne route dominates exposure of respiratory infection during close contact. *Building and Environment*, 176: 106859.
- Chen W, Qian H, Zhang N, et al. (2022). Extended short-range airborne transmission of respiratory infections. *Journal of Hazardous Materials*, 422: 126837.
- Coroneo MT, Collignon PJ (2021). SARS-CoV-2: Eye protection might be the missing key. *The Lancet Microbe*, 2: e173–e174.
- Craven BA, Settles GS (2006). A computational and experimental investigation of the human thermal plume. *Journal of Fluids Engineering*, 128: 1251–1258.
- de Dear RJ, Arens E, Hui Z, et al. (1997). Convective and radiative heat transfer coefficients for individual human body segments. *International Journal of Biometeorology*, 40: 141–156.
- Duguid JP (1946). The size and the duration of air-carriage of respiratory droplets and droplet-nuclei. *Epidemiology & Infection*, 44: 471–479.
- Dunnett SJ, Ingham DB (1988). An empirical model for the aspiration efficiencies of blunt aerosol samplers orientated at an angle to the oncoming flow. *Aerosol Science and Technology*, 8: 245–264.
- Gao NP, Niu JL (2005). CFD study of the thermal environment around a human body: a review. *Indoor and Built Environment*, 14: 5–16.
- Jia W, Wei J, Cheng P, et al. (2022). Exposure and respiratory infection risk via the short-range airborne route. *Building and Environment*, 219: 109166.
- Lei H, Xiao S, Cowling BJ, et al. (2020). Hand hygiene and surface cleaning should be paired for prevention of fomite transmission. *Indoor Air*, 30: 49–59.
- Li Y, Leung GM, Tang JW, et al. (2007). Role of ventilation in airborne transmission of infectious agents in the built environment—A multidisciplinary systematic review. *Indoor Air*, 17: 2–18.
- Li Y (2021). Basic routes of transmission of respiratory pathogens—A new proposal for transmission categorization based on respiratory spray, inhalation, and touch. *Indoor Air*, 31: 3–6.

- Li Y, Qian H, Hang J, et al. (2021). Probable airborne transmission of SARS-CoV-2 in a poorly ventilated restaurant. *Building and Environment*, 196: 107788.
- Li X, Ai Z, Ye J, et al. (2022a). Airborne transmission during short-term events: Direct route over indirect route. *Building Simulation*, 15: 2097–2110.
- Li Y, Cheng P, Jia W (2022b). Poor ventilation worsens short-range airborne transmission of respiratory infection. *Indoor Air*, 32: e12946.
- Lindsay WG, Blachere FM, Thewlis RE, et al. (2010). Measurements of airborne influenza virus in aerosol particles from human coughs. *PLoS One*, 5: e15100.
- Liu L, Li Y, Nielsen PV, et al. (2017). Short-range airborne transmission of expiratory droplets between two people. *Indoor Air*, 27: 452–462.
- Liu Z, Zhu H, Song Y, et al. (2022). Quantitative distribution of human exhaled particles in a ventilation room. *Building Simulation*, 15: 859–870.
- Miller SL, Nazaroff WW, Jimenez JL, et al. (2021). Transmission of SARS-CoV-2 by inhalation of respiratory aerosol in the Skagit Valley Chorale superspreading event. *Indoor Air*, 31: 314–323.
- Milton DK (2020). A Rosetta stone for understanding infectious drops and aerosols. *Journal of the Pediatric Infectious Diseases Society*, 9: 413–415.
- Morawska L, Johnson GR, Ristovski ZD, et al. (2009). Size distribution and sites of origin of droplets expelled from the human respiratory tract during expiratory activities. *Journal of Aerosol Science*, 40: 256–269.
- Morawska L, Tang JW, Bahnfleth W, et al. (2020). How can airborne transmission of COVID-19 indoors be minimised? *Environment International*, 142: 105832.
- Mui KW, Wong LT, Wu CL, et al. (2009). Numerical modeling of exhaled droplet nuclei dispersion and mixing in indoor environments. *Journal of Hazardous Materials*, 167: 736–744.
- Ou C, Hu S, Luo K, et al. (2022). Insufficient ventilation led to a probable long-range airborne transmission of SARS-CoV-2 on two buses. *Building and Environment*, 207: 108414.
- Popov TA, Dunev S, Kralimarkova TZ, et al. (2007). Evaluation of a simple, potentially individual device for exhaled breath temperature measurement. *Respiratory Medicine*, 101: 2044–2050.
- Prather KA, Marr LC, Schooley RT, et al. (2020). Airborne transmission of SARS-CoV-2. *Science*, 370: 303–304.
- Somsen GA, van Rijn C, Kooij S, et al. (2020). Small droplet aerosols in poorly ventilated spaces and SARS-CoV-2 transmission. *The Lancet Respiratory Medicine*, 8: 658–659.
- Sun W, Ji J (2007). Transport of droplets expelled by coughing in ventilated rooms. *Indoor and Built Environment*, 16: 493–504.
- Wei J, Li Y (2015). Enhanced spread of expiratory droplets by turbulence in a cough jet. *Building and Environment*, 93: 86–96.
- Wells WF (1934). On air-borne infection: study II. Droplets and droplet nuclei. *American Journal of Epidemiology*, 20: 611–618.
- WHO (2020a). Transmission of SARS-CoV-2: Implications for infection prevention precautions—Scientific Brief, 9 July 2020. Available at <https://www.who.int/news-room/commentaries/detail/transmission-of-sars-cov-2-implications-for-infection-prevention-precautions>. Accessed 23 July 2022.
- WHO (2020b). Modes of transmission of virus causing COVID-19: implications for IPC precaution recommendations—Scientific Brief, 29 March 2020. Available at <https://www.who.int/news-room/commentaries/detail/modes-of-transmission-of-virus-causing-covid-19-implications-for-ipc-precaution-recommendations>. Accessed 23 July 2022.
- WHO (2021). Coronavirus disease (COVID-19): How is it transmitted? Available at <https://www.who.int/emergencies/diseases/novel-coronavirus-2019/question-and-answers-hub/q-a-detail/coronavirus-disease-covid-19-how-is-it-transmitted>. Accessed 23 July 2022.
- Xie X, Li Y, Chwang AY, et al. (2007). How far droplets can move in indoor environments—Revisiting the Wells evaporation-falling curve. *Indoor Air*, 17: 211–225.
- Xu J, Psikuta A, Li J, et al. (2019). Influence of human body geometry, posture and the surrounding environment on body heat loss based on a validated numerical model. *Building and Environment*, 166: 106340.
- Yakhot V, Orszag SA (1986). Renormalization group analysis of turbulence. I. Basic theory. *Journal of Scientific Computing*, 1: 3–51.
- Zhang N, Chen W, Chan PT, et al. (2020a). Close contact behavior in indoor environment and transmission of respiratory infection. *Indoor Air*, 30: 645–661.
- Zhang N, Jia W, Wang P, et al. (2020b). Most self-touches are with the nondominant hand. *Scientific Reports*, 10: 10457.
- Zhang N, Chen X, Jia W, et al. (2021). Evidence for lack of transmission by close contact and surface touch in a restaurant outbreak of COVID-19. *The Journal of Infection*, 83: 207–216.
- Zhao P, Li Y, Tsang TL, et al. (2018). Equilibrium of particle distribution on surfaces due to touch. *Building and Environment*, 143: 461–472.
- Zhao P, Chan PT, Gao Y, et al. (2019). Physical factors that affect microbial transfer during surface touch. *Building and Environment*, 158: 28–38.
- Zhu S, Kato S, Yang JH (2006). Study on transport characteristics of saliva droplets produced by coughing in a calm indoor environment. *Building and Environment*, 41: 1691–1702.